JRP-1

Pseudoscalar contributions to the muon g-2 from lattice QCD and BES-III data

St. Goar, 12.06.2025

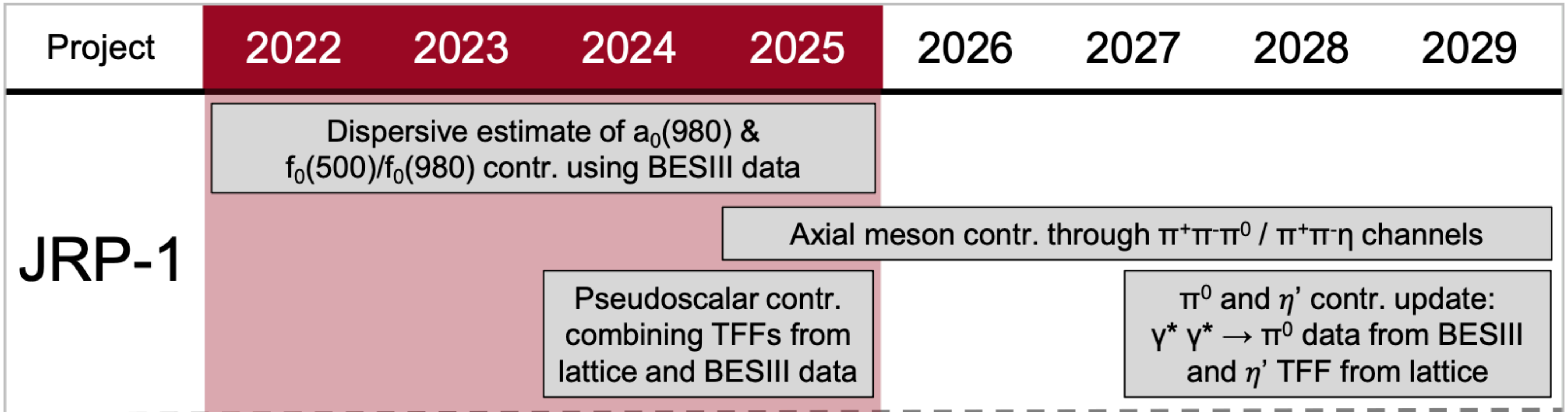

JRP-1

Pseudoscalar contributions to the muon g-2 from lattice QCD and BES-III data

St. Goar, 12.06.2025

HLBL SUMMARY — 1.WP

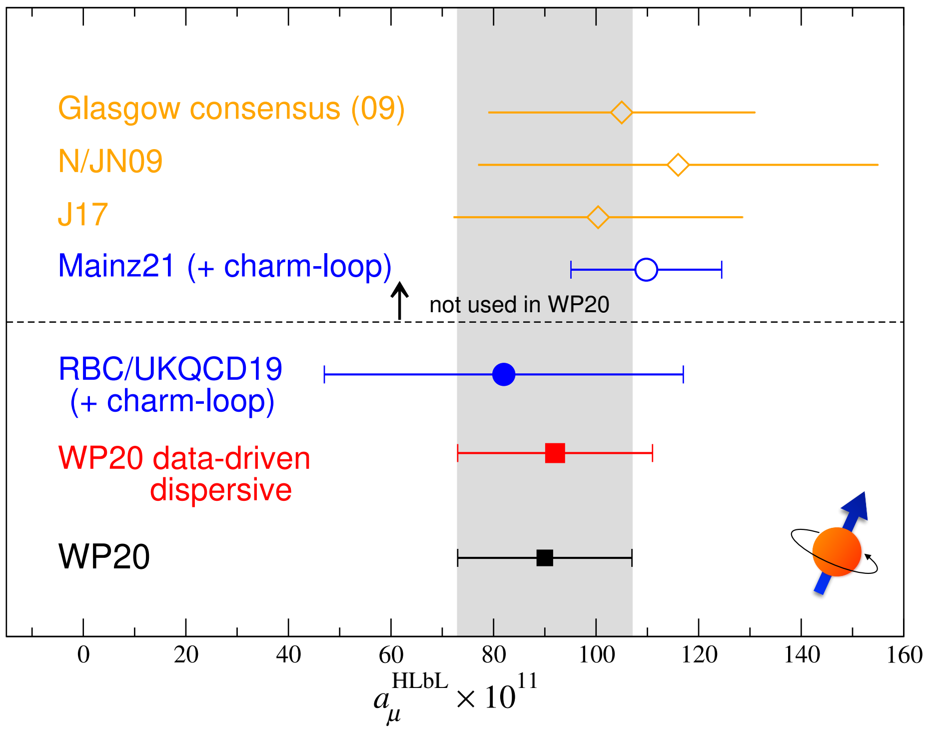

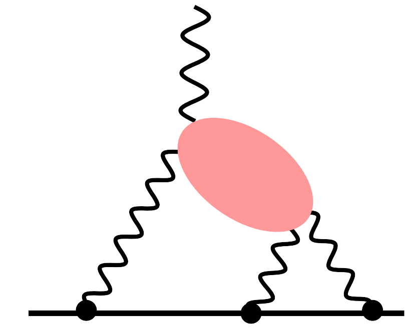

$$a_\mu^{\text{HLbL}}(\text{phenomenology + lattice QCD}) + a_\mu^{\text{HLbL, NLO}} = 92(18) \times 10^{-11}$$

- Data-driven and lattice QCD predictions are consistent

$\Longrightarrow$ 10% uncertainty feasible (by 2025) [Snowmass ’21]

Contribution	PdRV(09) [471]	N/JN(09) [472, 573]	J(17) [27]	Our estimate
π^0, η, η'-poles	114(13)	99(16)	95.45(12.40)	93.8(4.0)
π, K-loops/boxes	−19(19)	−19(13)	−20(5)	−16.4(2)
S-wave $\pi\pi$ rescattering	−7(7)	−7(2)	−5.98(1.20)	−8(1)
subtotal	88(24)	73(21)	69.5(13.4)	69.4(4.1)
scalars	–	–	–	− 1(3)
tensors	–	–	1.1(1)	
axial vectors	15(10)	22(5)	7.55(2.71)	6(6)
u, d, s-loops / short-distance	–	21(3)	20(4)	15(10)
c-loop	2.3	–	2.3(2)	3(1)
total	105(26)	116(39)	100.4(28.2)	92(19)

Table 15: Comparison of two frequently used compilations for HLbL in units of 10^{-11} from 2009 and a recent update with our estimate. PdRV = Prades, de Rafael, Vainshtein (“Glasgow consensus”); N/JN = Nyffeler / Jegerlehner, Nyffeler; J = Jegerlehner.

HLBL SUMMARY — 1.WP

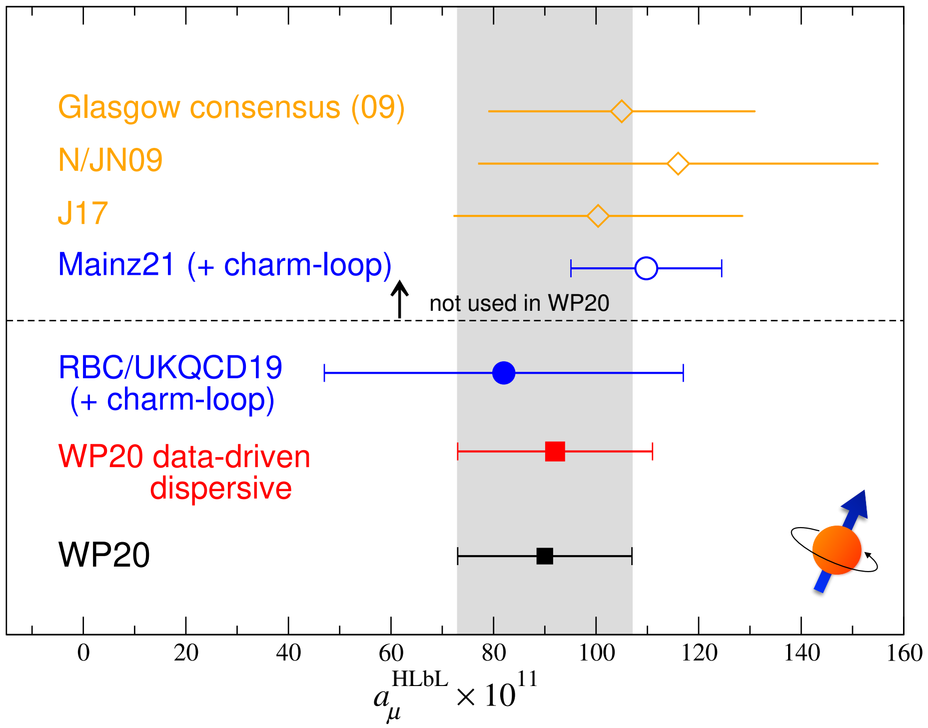

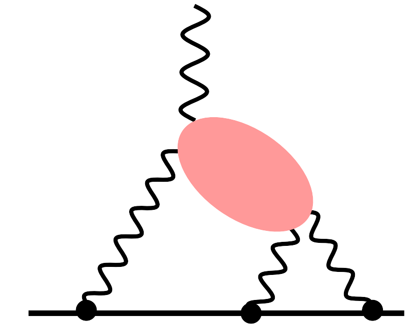

$$a_\mu^{\mathrm{HLbL}}(\text{phenomenology + lattice QCD}) + a_\mu^{\mathrm{HLbL,\,NLO}} = 92(18) \times 10^{-11}$$

- Data-driven and lattice QCD predictions are consistent

$\Longrightarrow$ 10% uncertainty feasible (by 2025) [Snowmass '21] ✅

Contribution	PdRV(09) [471]	N/JN(09) [472, 573]	J(17) [27]	Our estimate
π^0, η, η'-poles	114(13)	99(16)	95.45(12.40)	93.8(4.0)
π, K-loops/boxes	−19(19)	−19(13)	−20(5)	−16.4(2)
S-wave $\pi\pi$ rescattering	−7(7)	−7(2)	−5.98(1.20)	−8(1)
subtotal	88(24)	73(21)	69.5(13.4)	69.4(4.1)
scalars	–	–	–	} − 1(3)
tensors	–	–	1.1(1)	}
axial vectors	15(10)	22(5)	7.55(2.71)	6(6)
u, d, s-loops / short-distance	–	21(3)	20(4)	15(10)
c-loop	2.3	–	2.3(2)	3(1)
total	105(26)	116(39)	100.4(28.2)	92(19)

Table 15: Comparison of two frequently used compilations for HLbL in units of 10^{-11} from 2009 and a recent update with our estimate. PdRV = Prades, de Rafael, Vainshtein ("Glasgow consensus"); N/JN = Nyffeler / Jegerlehner, Nyffeler; J = Jegerlehner.

PSEUDOSCALAR-POLE CONTRIBUTION

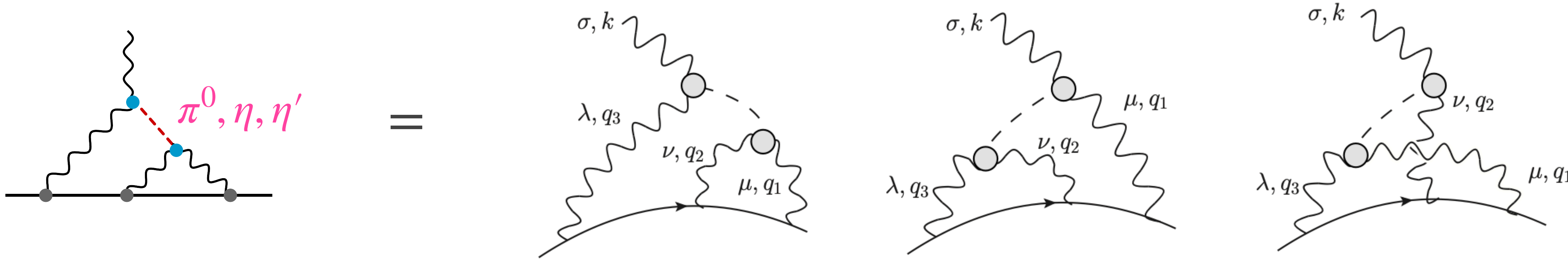

$$a_\mu^{P-\text{pole}} = \left(\frac{\alpha}{\pi}\right)^3 \int \mathrm{d}Q_1 \mathrm{d}Q_2 \mathrm{d}\tau \Big[w_1(Q_1, Q_2, \tau)\, F_{P\gamma^*\gamma^*}(-Q_1^2, -Q_3^2) F_{P\gamma^*\gamma}(-Q_2^2, 0)$$

$$+ w_2(Q_1, Q_2, \tau)\, F_{P\gamma^*\gamma^*}(-Q_1^2, -Q_2^2) F_{P\gamma^*\gamma}(-Q_3^2, 0) \Big]$$

on-shell pseudoscalar transition form factors (TFFs)

kernel functions are peaked at low energies

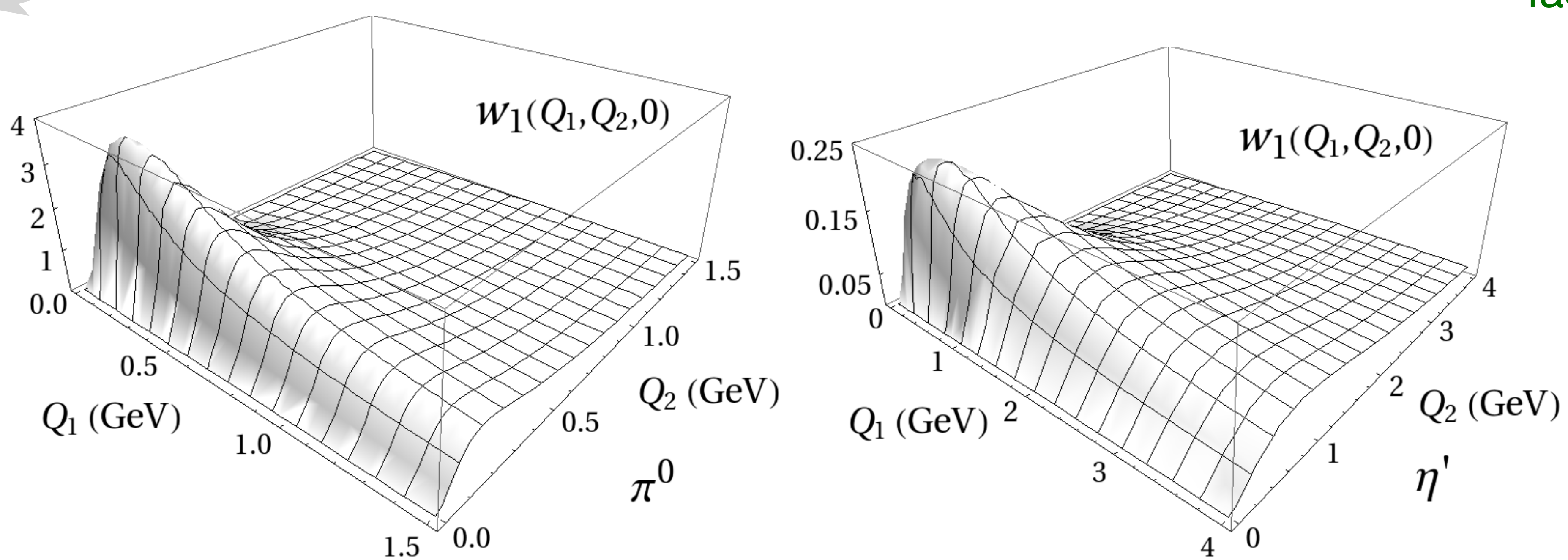

Figure 58: Weight function $w_1(Q_1, Q_2, 0)$ for π^0 (left) and η' (right); cf. Eq. (4.19). Reprinted from Ref. [19].

HLBL SUMMARY — 2.WP

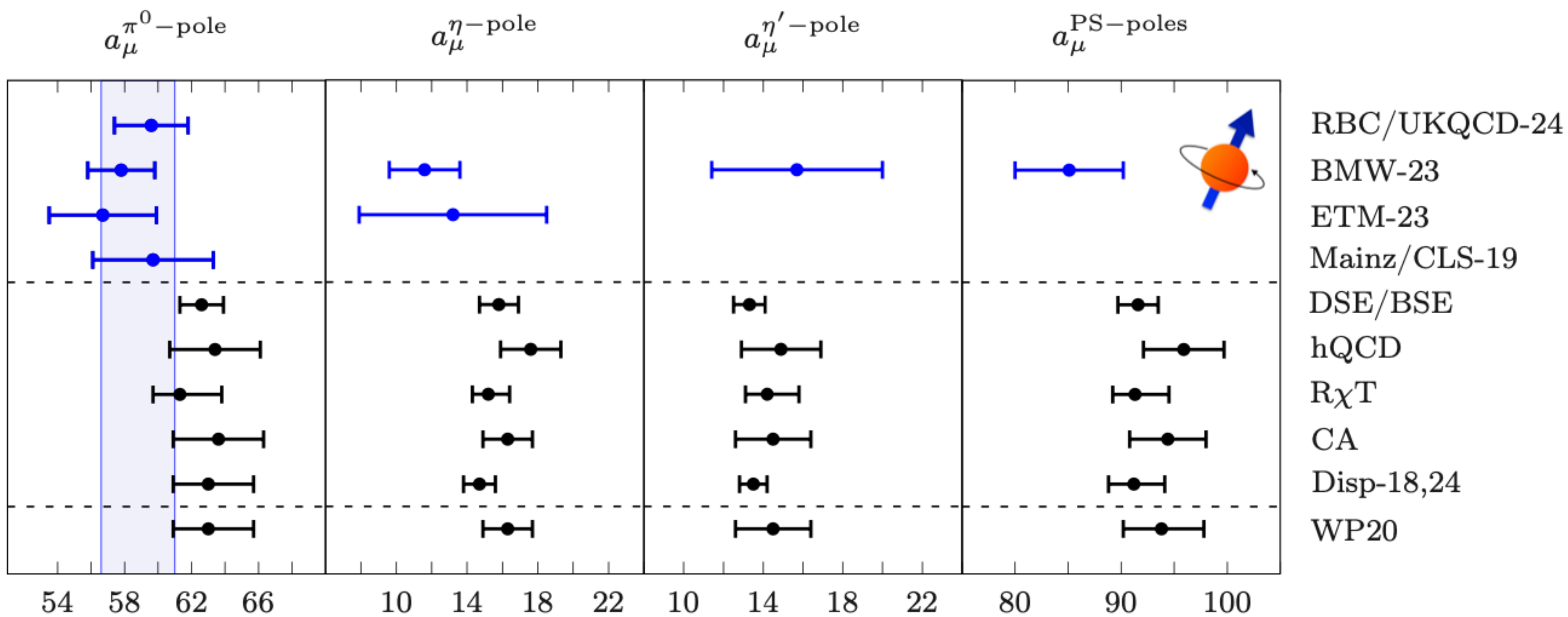

Figure 76: Summary of the lattice calculations (in blue) and of the approaches presented in Sec. 5, and comparison with the WP20 average. The blue band represents the lattice average for the pion-pole contribution.

lattice results are consistent with each other

$$a_\mu^{\pi^0\text{-pole}} = a_\mu^{\pi^0\text{-pole,conn}} \pm \left|a_\mu^{\pi^0\text{-pole,disc}}\right| = 58.8(1.1)_{\mathrm{stat}}(1.1)_{\mathrm{syst}}(1.6)_{\mathrm{disc}}[2.2]_{\mathrm{tot}} \times 10^{-11} \qquad \text{(lattice QCD average)}$$

	Dispersive [36, 55, 543, 545]	CA [34]	RχT [49]	hQCD [46]	DSE/BSE [37]
π^0	$63.0^{+2.7}_{-2.1}$	63.6(2.7)	$61.3^{+2.5}_{-1.6}$	63.4(2.7)	62.6(1.3)
η	14.7(9)	16.3(1.4)	$15.2^{+1.2}_{-0.9}$	17.6(1.7)	15.8(1.1)
η'	13.5(7)	14.5(1.9)	$14.2^{+1.6}_{-1.1}$	14.9(2.0)	13.3(8)
Sum	$91.2^{+2.9}_{-2.4}$	94.4(3.6)	$91.3^{+3.2}_{-2.1}$	95.9(3.8)	91.6(1.9)

Table 28: The pseudoscalar pole contributions to a_μ in units of 10^{-11} from the different approaches.

lattice and data-driven results are consistent at 1.5σ level

HLBL SUMMARY — 2. WP

Contribution	WP25	WP20
HVP LO (lattice)	7132(61)	7116(184)
HVP LO (e^+e^-, τ)	Table 5	6931(40)*
HVP NLO (e^+e^-)	−99.6(1.3)	−98.3(7)
HVP NNLO (e^+e^-)	12.4(1)	12.4(1)
HLbL (phenomenology)	103.3(8.8)	92(19)
HLbL NLO (phenomenology)	2.6(6)	2(1)
HLbL (lattice)	122.5(9.0)	82(35)
HLbL (phenomenology + lattice)	112.6(9.6)	90(17)
QED	116 584 718.8(2)	116 584 718.931(104)
EW	154.4(4)	153.6(1.0)
HVP (LO + NLO + NNLO)	7045(61)	6845(40)
HLbL (phenomenology + lattice + NLO)	115.5(9.9)	92(18)
Total SM Value	116 592 033(62)	116 591 810(43)

uncertainty
scaled by 1.5

Table 33: Comparison of the key results from this work (WP25), as given in Table 1, to the corresponding numbers from WP20 [1] (in units of 10^{-11}). Note that the "HLbL (lattice)" result from WP20 has been adapted to include the charm-loop contribution. The entry "HVP (LO + NLO + NNLO)" derives from HVP LO (lattice) [WP25] and HVP LO (e^+e^-) [WP20], respectively. The asterisk indicates that the LO HVP value from WP20 was based on e^+e^- data only, while in Table 5 we also include the current status for τ-based evaluations.

THE IDEA

- **Requirement:** Lattice QCD and data-driven evaluations of pion transition form factors (TFFs) are consistent with each other
- **Idea:** Combined analysis of lattice QCD and experimental data
- **Motivation:** further reduce (systematic and extrapolation) uncertainties
- Singly-virtual region:
  - New BES-III data at lower virtualities ($Q^2 \sim 0.2$ GeV^2) [talk by Christoph]
  - Larger systematic uncertainties for lattice QCD at $Q^2 < 0.5$ GeV^2
- Doubly-virtual region:
  - No experimental data for π [talk by Christoph]
  - 5 data points for η and 1 data point for η'

PION TFF — 2. WP

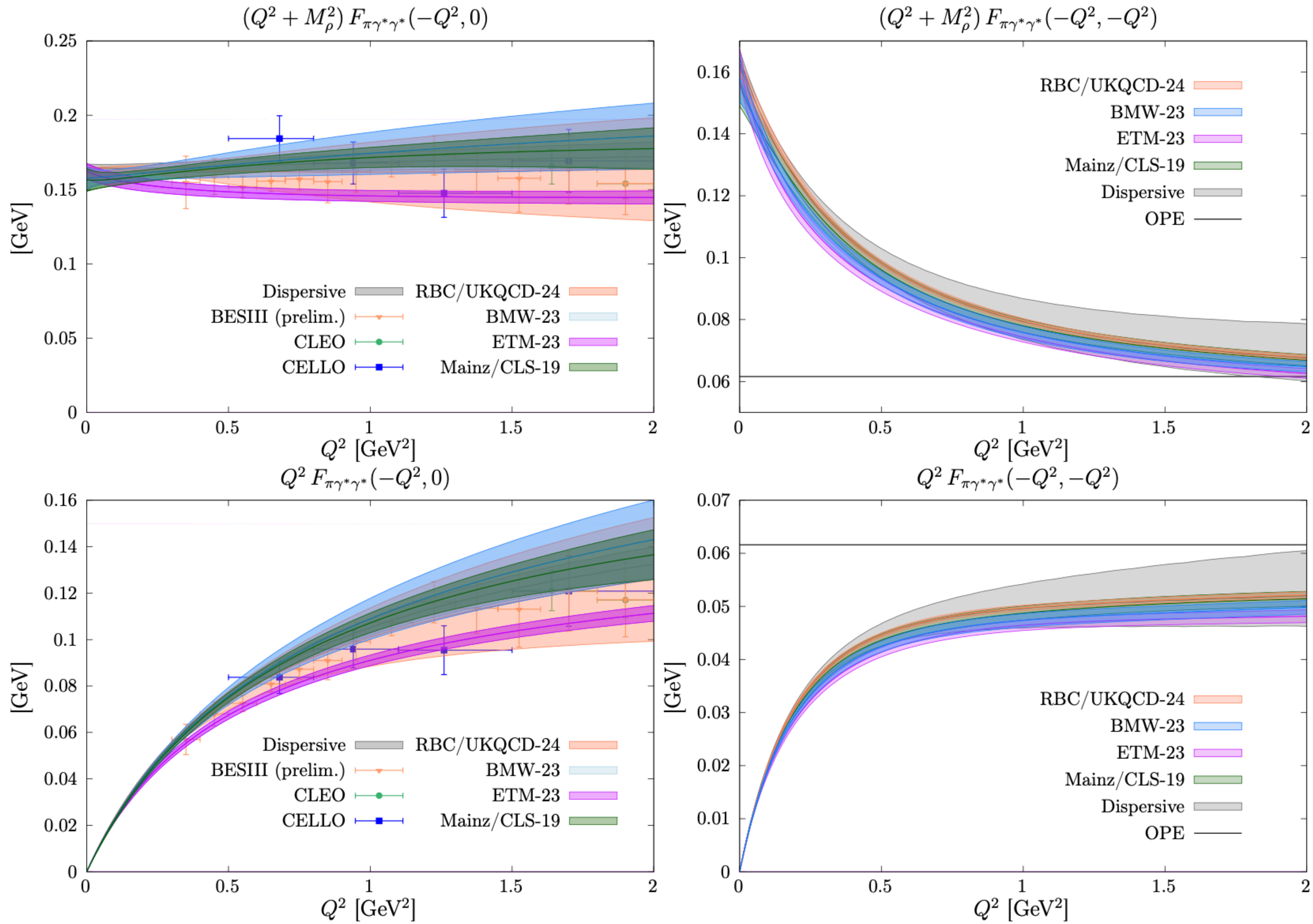

Figure 77: Comparison of lattice calculations [544, 571, 643, 706], the dispersive determination of Ref. [543], and experimental data (Refs. [559, 560] and preliminary BESIII data [1, 725]) for the single-virtual and the double-virtual π^0 TFF.

PION TFF — I. WP

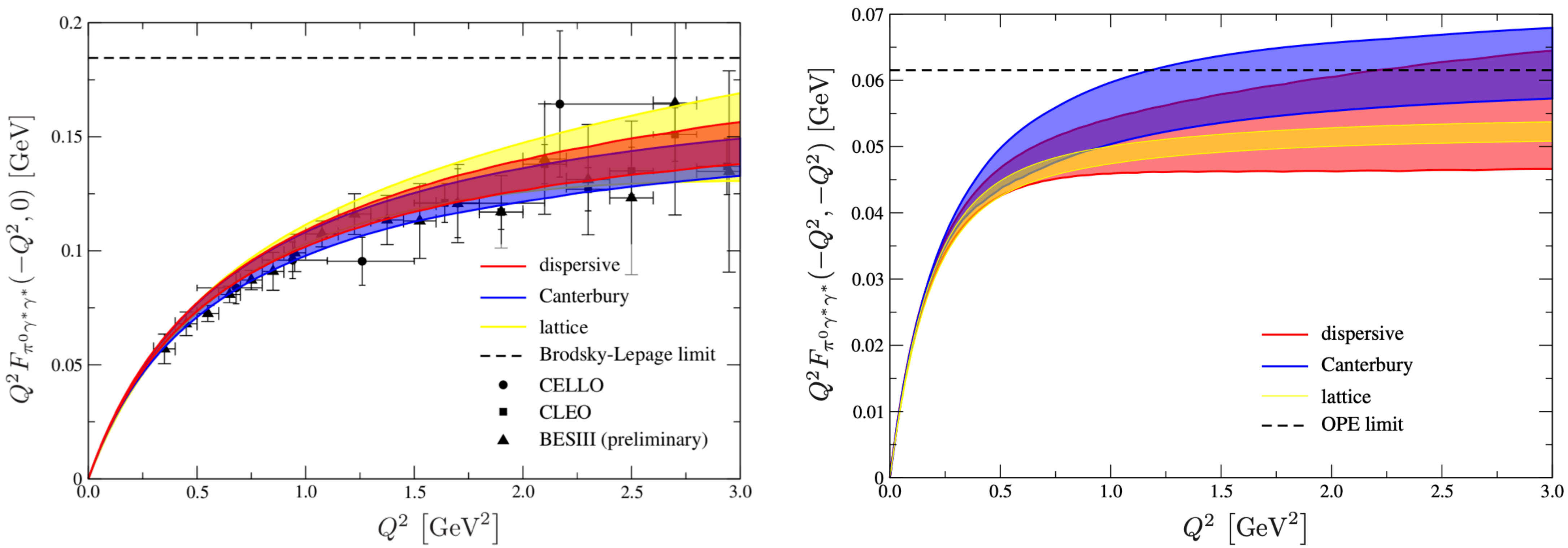

Figure 60: Comparison of the π^0 TFF from dispersion theory [21, 497] (red), CA [19] (blue), and lattice QCD [22] (yellow). We show both the singly- (left) and the doubly-virtual (right) form factors.

STATUS AND OUTLOOK

- Received data from Lattice Group
  [talking to Harvey, Jonna and Georg]
  - "Reproducing" fits analogously to 1607.08174
  - Understanding how to work with the data

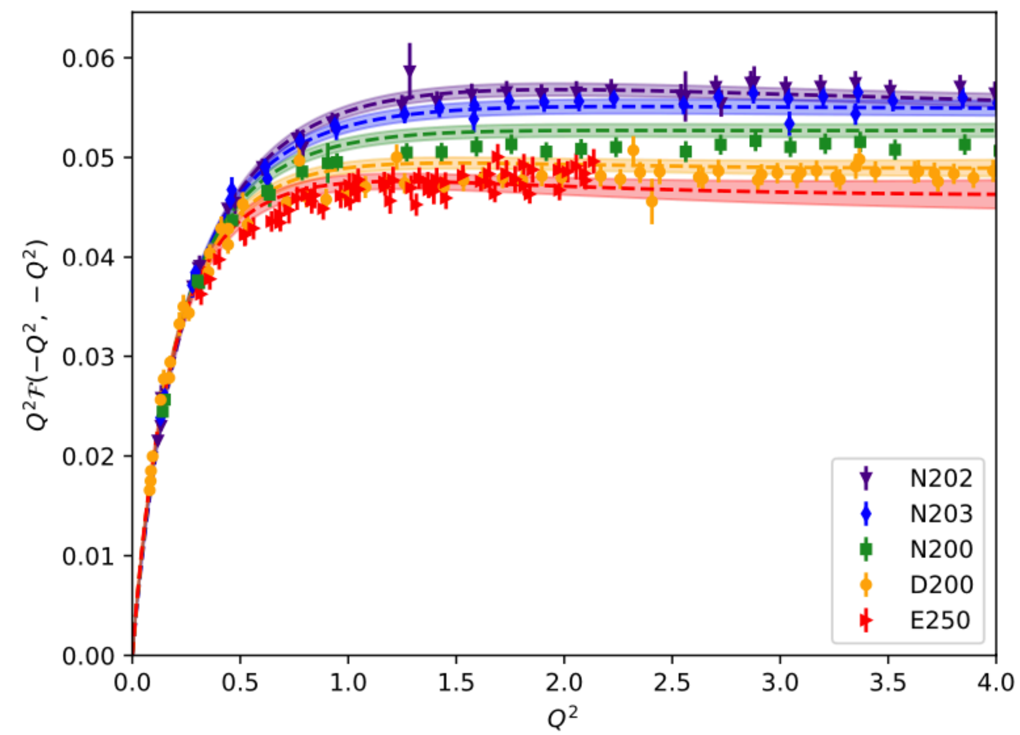

- Collected world data for space-like pion TFF
  - Waiting for BES-III data [talking to Christoph]
- Check consistency "lattice QCD" fit ↔ "experimental" data / fit
- Combined LMD+V fit of lattice QCD & experimental data
- No Mainz lattice QCD data from Mainz for η and η'
- Possible extensions: BChPT (Scherer et al.), time-like data, dispersive analysis

People

JRP-1: Pseudoscalar contributions to the muon g-2 from lattice QCD and BES-III data

- Naomi Danaheb Navarro Durán (master student since April)

  → first “naive” combined fit of LQCD and experimental pion TFF data;

- Vladyslava Sharkovska (present RU PhD, March - August ‘25)

  → cross check of fits; prepare possible extension to η and η'

- Sotiris Pitelis (future RU PhD, September ’25 - January ‘26)

  → fits beyond LMD+V; 3-particle production channel for Schwinger sum rule

- Timon Esser (master student)

  → spin-1 Compton scattering (LbL) sum rules, PWA

- **Vadim Lensky**

  → spin-1 Compton scattering (LbL) sum rules, PWA, …

Thank you for your attention!

PSEUDOSCALAR TFF

- On-shell pseudoscalar ($P = \pi^0, \eta, \eta'$) transition form factor $F_{P\gamma^*\gamma^*}(q_1^2, q_2^2)$:

$$i \int \mathrm{d}^4x \, e^{iq_1 \cdot x} \langle 0 | T\{j_\mu(x) j_\nu(0)\} | P(q_1 + q_2) \rangle = \epsilon_{\mu\nu\rho\sigma} q_1^\rho q_2^\sigma F_{P\gamma^*\gamma^*}(q_1^2, q_2^2)$$

- Normalized to the two-photon decay:

$$\Gamma(P \to \gamma\gamma) = \frac{\pi\alpha^2 M_P^3}{4} F_{P\gamma\gamma}^2, \qquad F_{P\gamma\gamma} = F_{P\gamma^*\gamma^*}(0,0)$$

- SDCs for pseudoscalar transition form factors (e.g., for the pion):
  - Chiral Anomaly: $F_{\pi^0\gamma\gamma}(0,0) = -\dfrac{1}{4\pi^2 f_\pi}$
  - Brodsky-Lepage limit: $\lim\limits_{Q^2 \to \infty} F_{\pi^0\gamma\gamma^*}(Q^2) = -\dfrac{2f_\pi}{Q^2}$
  - Symmetric pQCD limit: $\lim\limits_{Q^2 \to \infty} F_{\pi^0\gamma^*\gamma^*}(Q^2, Q^2) = -\dfrac{2f_\pi}{3Q^2}$

PION TFF — DISPERSIVE APPROACH

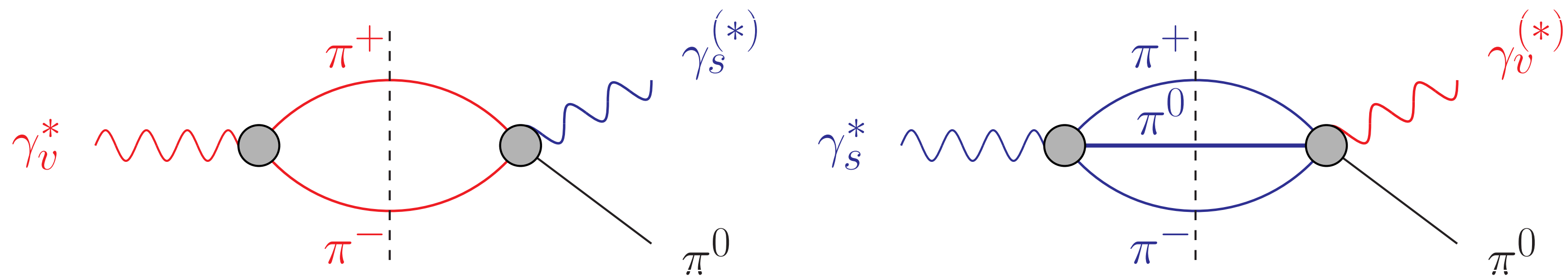

$$F_{\pi^0\gamma^*\gamma^*} = F^{\text{disp}}_{\pi^0\gamma^*\gamma^*} + F^{\text{eff}}_{\pi^0\gamma^*\gamma^*} + F^{\text{asym}}_{\pi^0\gamma^*\gamma^*}$$

M. Hoferichter, B.-L. Hoid, B. Kubis, S. Leupold, and S. P. Schneider, JHEP 10, 141 (2018)

- Dispersive part:

$$F^{\text{disp}}_{\pi^0\gamma^*\gamma^*}(-Q_1^2, -Q_2^2) = F^{\text{disp}}_{vs}(-Q_1^2, -Q_2^2) + F^{\text{disp}}_{vs}(-Q_2^2, -Q_1^2) = \frac{1}{\pi^2}\int_{4M_\pi^2}^{s_{iv}} \mathrm{d}x \int_{s_{\text{thr}}}^{s_{is}} \mathrm{d}y \, \frac{\rho(x,y)}{(x+Q_1^2)(y+Q_2^2)} + \{q_1 \leftrightarrow q_2\}$$

with $\rho(x,y) = \dfrac{(x/4 - M_\pi^2)^{3/2}}{12\pi\sqrt{x}} \mathrm{Im}[(F_\pi^V(x))^* f_1(x,y)]$

- Asymptotic contribution to ensure pQCD limit:

$$F^{\text{asym}}_{\pi^0\gamma^*\gamma^*}(-Q_1^2, -Q_2^2) = 2f_\pi \int_{s_m}^{\infty} \mathrm{d}x \frac{Q_1^2 Q_2^2}{(x+Q_1^2)^2(y+Q_2^2)^2}$$

- Effective pole ($M_{\text{eff}} \sim 1.5 - 2\,\text{GeV}$) parametrising heavier intermediate states:

$$F^{\text{eff}}_{\pi^0\gamma^*\gamma^*}(-Q_1^2, -Q_2^2) = \frac{g_{\text{eff}}}{4\pi^2 f_\pi} \frac{M_{\text{eff}}^4}{(M_{\text{eff}}^2 + Q_1^2)(M_{\text{eff}}^2 + Q_2^2)}$$

ETA & ETA' TFF

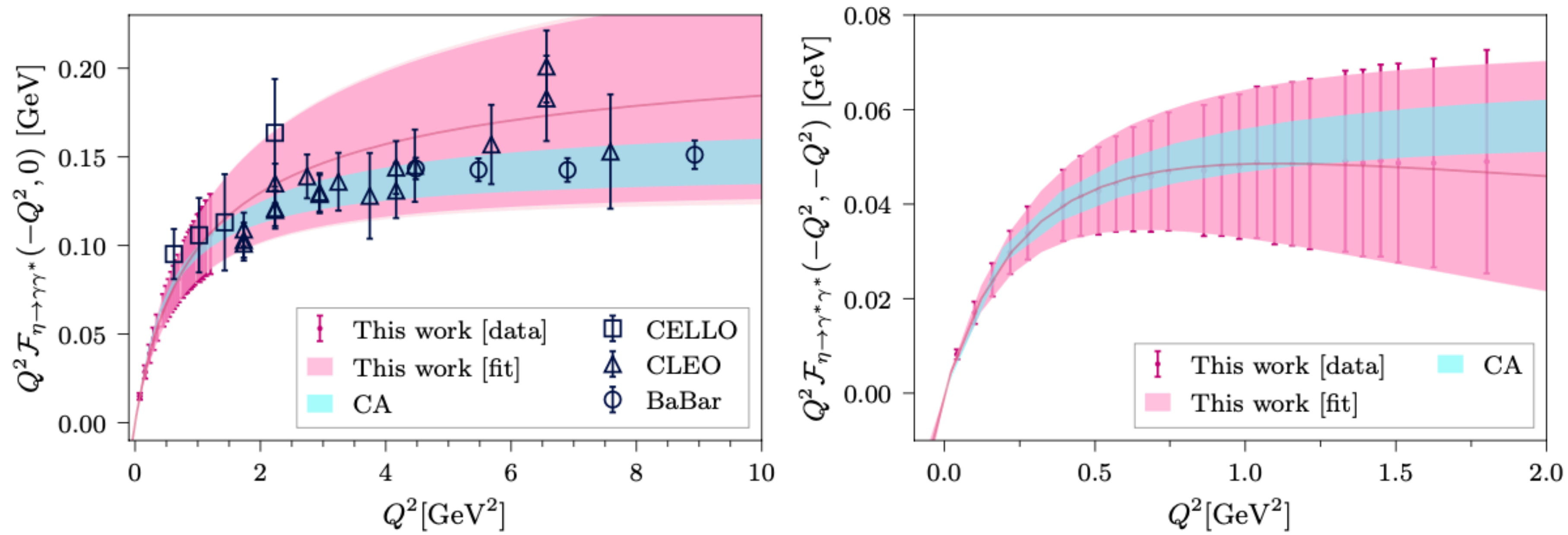

Figure 73: The η TFF from the ETM collaboration in the single-virtual (left) and double-virtual (right) kinematics [570]. The result, obtained at a single lattice spacing, is compared with experimental results and the Canterbury estimate (cyan bands).

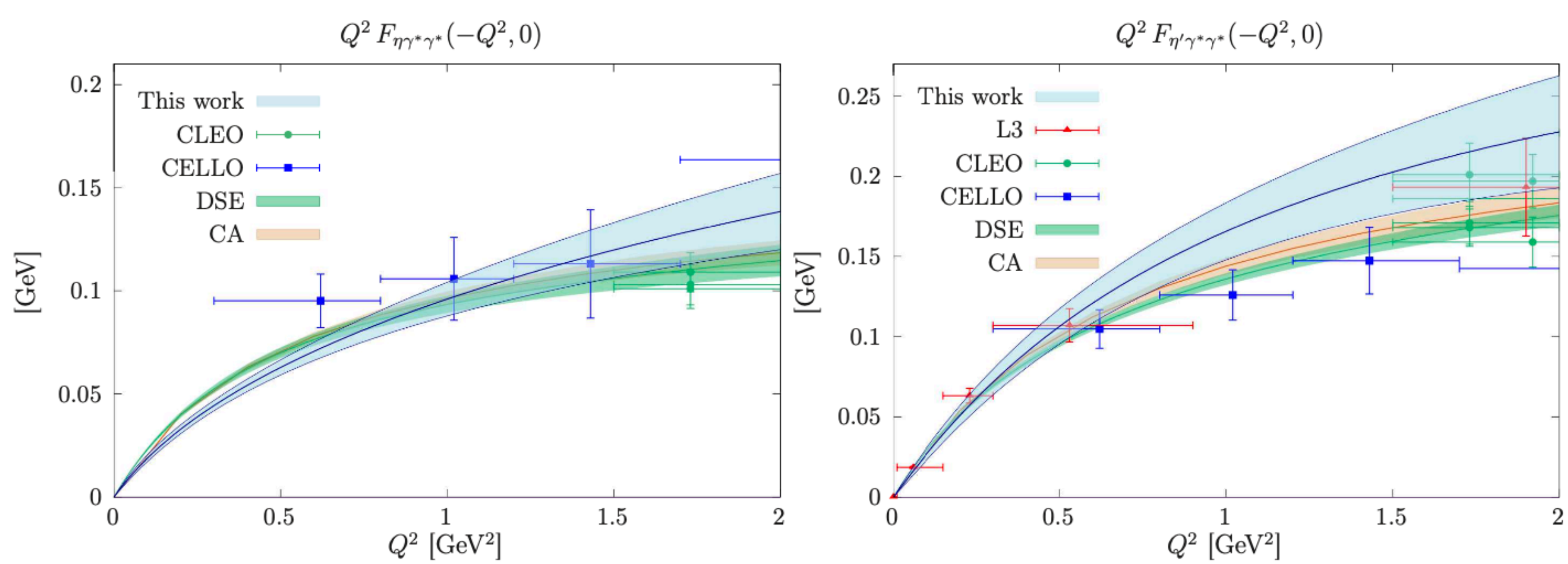

Figure 74: The η (left) and η' (right) single-virtual TFFs from the BMW collaboration at the physical point and in the continuum limit. The Canterbury approximant (CA) result is extracted from Ref. [34] and the Dyson–Schwinger equation (DSE) result comes from Ref. [37]. Measurements from CELLO [559], CLEO [560], and L3 [561] are shown for comparison. Figure from Ref. [571].

ETA & ETA' TFF

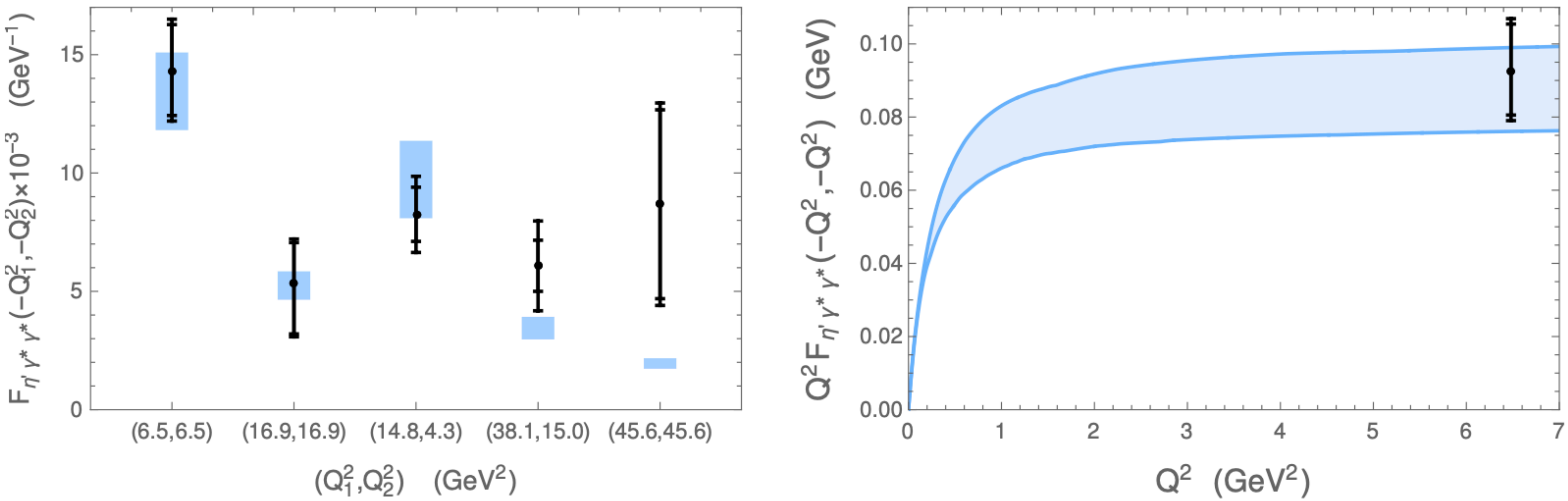

Figure 59: Left: BABAR data points [108] with statistical errors (inner bars) and statistical and systematic combined (outer bars) in black, together with the CA prediction including errors (blue bands). Right: The analogous plot for the diagonal $Q^2F_{\eta'\gamma^*\gamma^*}(-Q^2,-Q^2)$ TFF.

$$a_\mu^{\eta\text{-pole}} = 16.3(1.0)_{\text{stat}}(0.5)_{a_{P;1,1}}(0.9)_{\text{sys}} \times 10^{-11} \rightarrow 16.3(1.4)\times10^{-11}$$

$$a_\mu^{\eta'\text{-pole}} = 14.5(0.7)_{\text{stat}}(0.4)_{a_{P;1,1}}(1.7)_{\text{sys}} \times 10^{-11} \rightarrow 14.5(1.9)\times10^{-11}$$